Dynamic microscopy of nanoscale cluster growth at the solid–liquid interface

M. J. WILLIAMSON[1], R. M. TROMP[2], P. M. VEREECKEN[2], R. HULL[1] AND F. M. ROSS*[2]

[1] School of Engineering and Applied Science, University of Virginia, Charlottesville, Virginia 22903, USA

[2] IBM T. J. Watson Research Center, Yorktown Heights, New York 10598, USA

*e-mail: fmross@us.ibm.com

Published online: 20 July 2003; doi:10.1038/nmat944

Dynamic processes at the solid–liquid interface are of key importance across broad areas of science and technology. Electrochemical deposition of copper, for example, is used for metallization in integrated circuits, and a detailed understanding of nucleation, growth and coalescence is essential in optimizing the final microstructure. Our understanding of processes at the solid–vapour interface has advanced tremendously over the past decade due to the routine availability of real-time, high-resolution imaging techniques yielding data that can be compared quantitatively with theory[1–3]. However, the difficulty of studying the solid–liquid interface leaves our understanding of processes there less complete. Here we analyse dynamic observations—recorded *in situ* using a novel transmission electron microscopy technique—of the nucleation and growth of nanoscale copper clusters during electrodeposition. We follow in real time the evolution of individual clusters, and compare their development with simulations incorporating the basic physics of electrodeposition during the early stages of growth. The experimental technique developed here is applicable to a broad range of dynamic phenomena at the solid–liquid interface.

Electrochemically deposited Cu films have been successfully developed for interconnects in integrated circuits, but continuing miniaturization requires us to deepen our understanding of nucleation, growth and coalescence, particularly in thin films and on polycrystalline substrates[4]. Even for electrodeposition of Cu on Au, a well-studied model system[5–11], fundamental questions remain. The only method of following nucleation and growth—processes that can take place over milliseconds—is indirectly, by measurement of the current transient and analysis based on electrochemical models[12–14]. In many systems, up to several orders of magnitude difference have been found between parameters obtained from current transient analysis and from post-growth microscopy[15]. Clearly, for electrochemical systems there is a great need for a technique that can image growth with good temporal and spatial resolution, and which can be used to measure the entire growth process for many clusters simultaneously. Electron microscopy fulfils some of these requirements, but although its use for growth processes under vacuum has become routine over the past decade, similar studies in liquid environments have not been possible, so far being limited to liquid inclusions or low-vapour-pressure liquids[16–18]. Scanning probe microscopy allows detailed structural measurements during liquid phase growth[5–10,19–22], but, because it requires typically

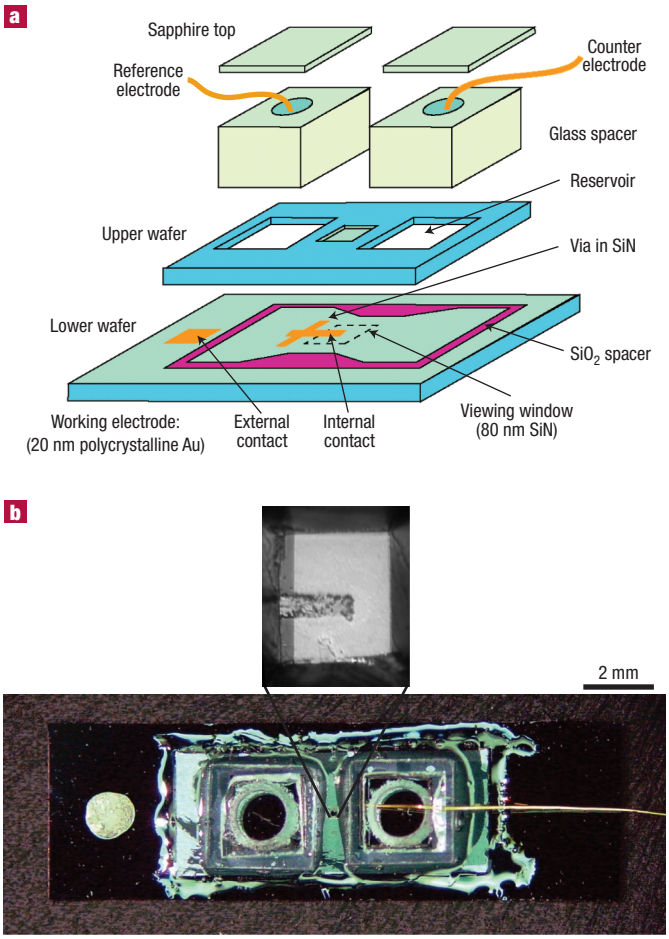

Figure 1 The liquid cell. a, Components of the cell. The viewing window is enlarged for clarity. **b**, Photograph of a two-electrode cell with an optical micrograph of the viewing window.

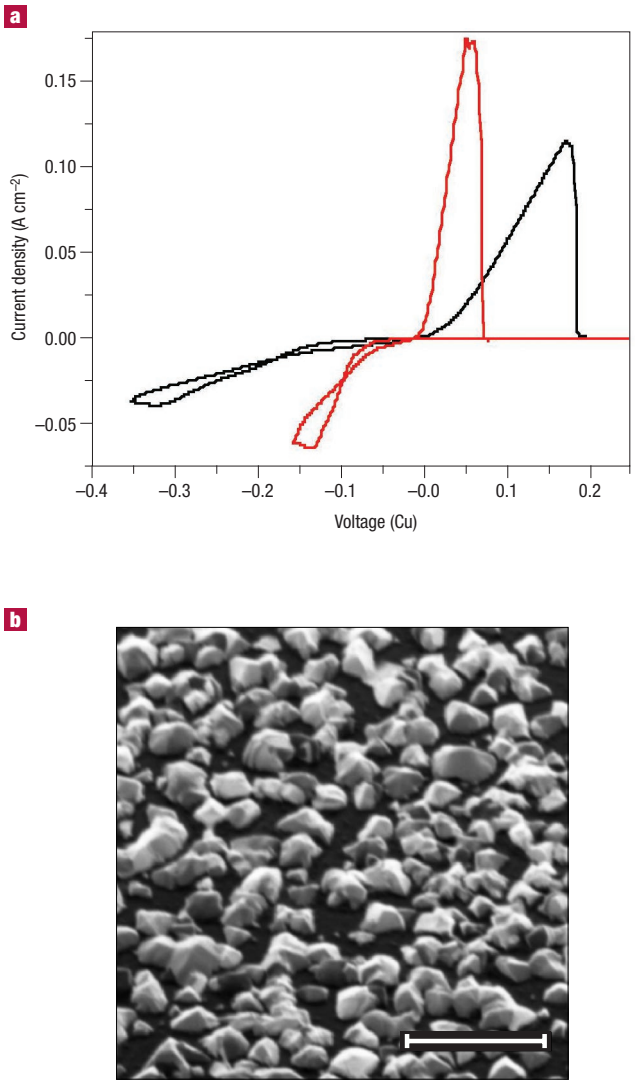

Figure 2 Electrodeposition in a small volume. a, Cyclic voltammograms: Black curve: electrodeposition of Cu on polycrystalline Au, recorded in the liquid cell using a Cu reference electrode. The scan rate was 25 mV s^{-1} and the electrolyte contained 0.2 M $CuSO_4$ + 0.05 M H_2SO_4. Red curve: electrodeposition in a large volume of the same electrolyte measured using a Luggin capillary reference electrode. The current density was calculated using the cell's measured electrode area of 210 μm × 10 μm. The variation in peak potential and the slightly different peak current density are due to the ohmic drop over the solution in the cell's narrow channel. **b**, Copper clusters of density 6.5×10^8 cm^{-2} formed after galvanostatic deposition in a cell at 5 mA cm^{-2} (total current 0.1 μA) for 4 s. The image was recorded with a focused ion beam (FEI 200 TEM) using secondary-electron contrast. X-ray diffraction confirms the deposit as polycrystalline Cu. Scale bar 2 μm.

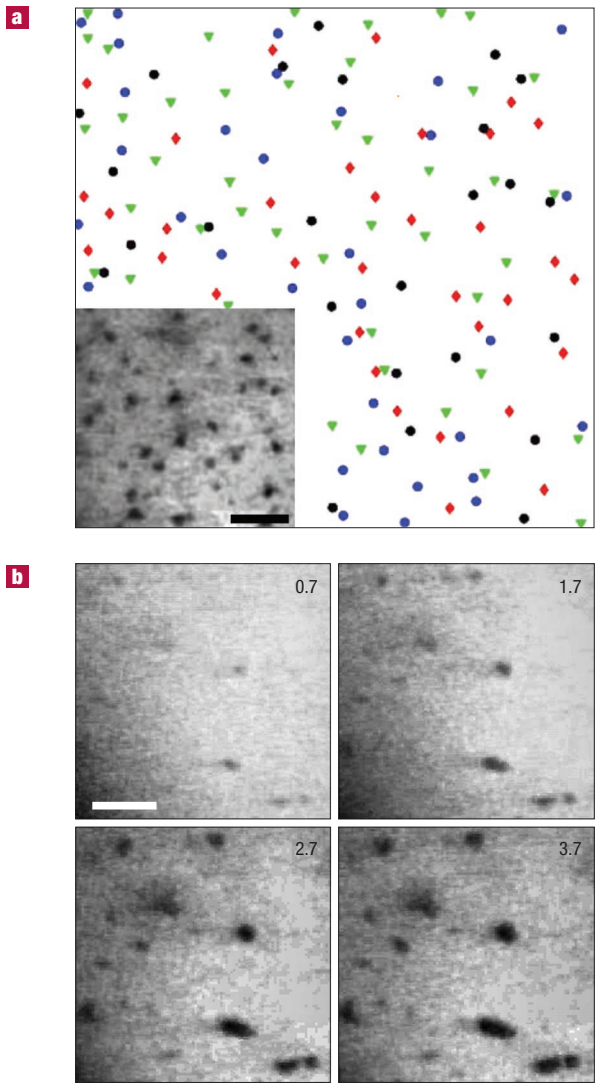

Figure 3 Cluster nucleation and growth observed *in situ*. a, The centre-of-mass positions of Cu clusters during four deposition experiments (different colours) on the same area of electrode. Galvanostatic deposition at 50 mA cm^{-2} was carried out in 0.3 M $CuSO_4$. Inset is the micrograph that corresponds to the black circles. Scale bar 500 nm. **b**, Small regions extracted from a video recorded during deposition at 5 mA cm^{-2}. The images were acquired at the times shown (in seconds) after current flow began. Scale bar 500 nm.

30 seconds per frame, generally does not resolve the subsecond processes that dominate the initial stages of growth. Fast acquisition techniques[23,24] enable reactions at step edges to be imaged at several frames per second, affording great insight into kink dynamics during growth on single-crystal substrates. However, this has not been extended to three-dimensional (Volmer–Weber) growth, or to more general substrates. Furthermore, tip effects may be significant[21]. X-ray diffraction[11,25] and Rutherford backscattering[26], with limited lateral resolution, have been confined to layer-by-layer growth on homogeneous substrates.

Here we present a real-time study of the growth of Cu clusters, using a novel technique capable of imaging reactions at the solid–liquid interface with a time resolution of 30 images per second (video rate), over a large area (several micrometres square), and at a spatial resolution of around 5 nm. Controlled deposition is carried out in a transmission electron microscope (TEM) so that established TEM imaging and analysis techniques can be used. The reaction takes place in a cell in which electrolyte is confined in an electron-transparent layer (Fig. 1). By observing deposition in real time, we can apply simple models to understand the key processes involved in nucleation and cluster growth.

An important initial question is whether electrodeposition in the restricted volume available in the cell faithfully mimics the standard process. In Fig. 2a we compare cyclic voltammograms recorded in the TEM cell with data from a larger electrochemical cell. Both cases show typical current peaks for diffusion-limited deposition and stripping of

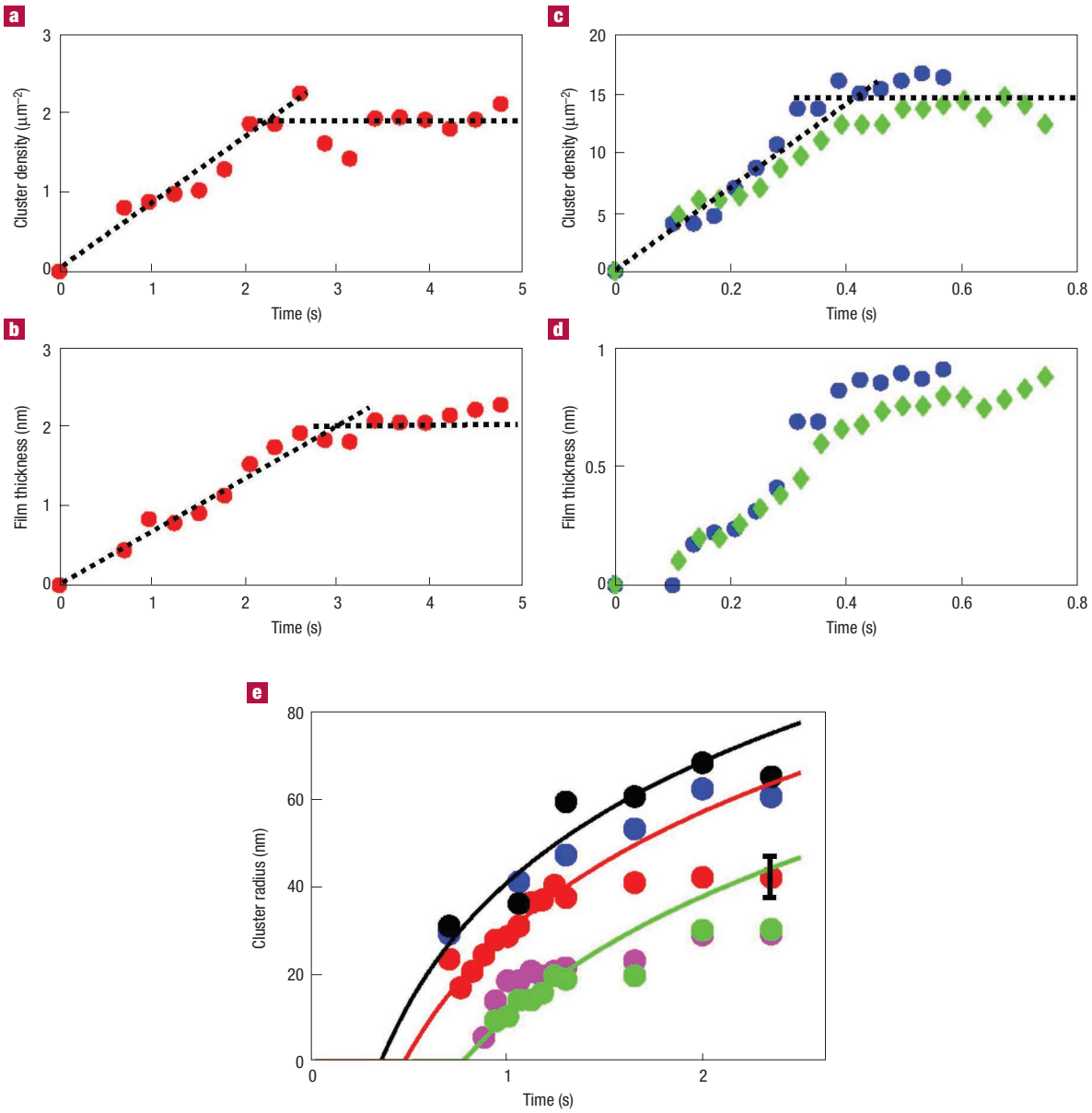

Figure 4 Individual cluster growth kinetics. a, Number density of clusters versus time during deposition at 5 mA cm^{-2}. The dotted lines suggest a constant nucleation rate lasting 2.5 seconds followed by almost zero additional nucleation. The initial nucleation rate is 2.5×10^8 cm^{-2} sec^{-1}, the final nucleus density $N_0 = 1.8 \times 10^8$ cm^{-2}, and the nucleation rate constant $k_n = 0.5$ s^{-1}. **b**, Average film thickness (that is, total cluster volume per unit area) calculated assuming that clusters are hemispherical. The dotted lines show an initially steady growth rate, which decreases after 3 s. The initial growth rate is within a factor of two of the rate expected from the average current density. **c**,**d**, Data corresponding to **a** and **b** but for deposition at 50 mA cm^{-2}. Two separate experiments are shown in different colours. In this case the initial nucleation rate is 2×10^9 cm^{-2} s^{-1}, $N_0 = 1.5 \times 10^9$ cm^{-2}, $k_n = 2$ s^{-1} and growth slows after 0.4 s. As expected, the higher growth rate leads to a greater nucleus density. **e**, The radii of several individual clusters in **a** and **b** fitted by the simulation described in the text, showing good fit at small times; beyond 1.5–2s, growth is limited by depletion in the liquid, which is not included in the simulation.

Cu. The similar current density suggests that deposition occurs only on the electrode and not elsewhere in the TEM cell, and *ex situ* examination confirms that three-dimensional (3D) clusters grow uniformly over the electrode (Fig. 2b).

We first investigated preferred nucleation sites for individual Cu clusters by examining an area of the electrode after four separate deposition experiments, with the Cu stripped between experiments (Fig. 3a). Each time, nuclei appear in different positions with no evident correlation. Nucleation of Cu on Au is known to occur preferentially at steps[10]. In our experiments, the grain size in the electrode (15 nm) is much smaller than the separation between nuclei (400 nm), so the density of surface defects potentially available (steps, grain boundaries and triple points) is much higher than the actual nucleus density. Thus the uncorrelated arrangement in Fig. 3a shows that nucleation is not dominated by a small population of preferred sites. If many sites have similar nucleation probability, we may be seeing the blocking of potential sites by the diffusion field of a previously formed cluster, a situation similar to homogeneous nucleation.

We now consider time-resolved data. Video sequences recorded during galvanostatic deposition are provided as Supplementary Information, and extracted images and data are shown here in Figs 3b and 4. Progressive nucleation and diffusion-limited 3D growth of Cu on Au was previously inferred from current transient measurements, which average over all nuclei and over the entire area[10,13,27]. The time dependence in Fig. 4a is consistent with this expected growth mode, and the data yield average parameters, such as nucleation rate constant, which are within the range cited in literature. However, by following the evolution of individual clusters, rather than averaged ensembles, we can compare with the progressive nucleation and 3D growth model in more detail (Fig. 4e). Galvanostatic conditions have not been treated theoretically in detail and we therefore derive below a simple model for comparison with the data.

After initial charging of the electrical double layer, and after formation of the first nuclei (both within 25 ms of starting growth and thus unobservable) the growth of each cluster becomes limited by its share of the total current I_o. For the j^{th} cluster, of volume V_j, Faraday's law gives

$$V_j(t) = \{M/(n\mathrm{F}\rho)\}\int_{t_j}^{t} I_j(t)\,\mathrm{d}t, \quad (1)$$

where M is the molar mass and ρ the density of copper, $n = 2$ electrons per ion, F is Faraday's constant, t_j is the time of nucleation of cluster j and $I_j(t)$ is the current received by cluster j. As long as there is no significant depletion of the solution, growth is surface-reaction limited and the current is shared between clusters according to their surface areas:

$$I_j(t) = I_o A_j(t)/\Sigma A_i(t), \quad (2)$$

where A_j is the surface area of cluster j; $A_j = (18\pi)^{1/3} V_j^{2/3}$ for hemispherical clusters.

Results from a simulation based on equations (1) and (2) are shown in Fig. 4e. Even though this simple model does not include convection or diffusion, it nevertheless provides a good match for cluster growth kinetics for early growth, up to ~2 s. This is significant in allowing calculations of cluster-size distribution, important in understanding film uniformity at coalescence. At later times, we expect slower, diffusion-limited kinetics due to depletion of ions in the solution. A reduction in growth rate is indeed seen after ~2 s (Fig. 4e), but due to the uncertainties in modelling diffusion in the confined volume (see below), this regime was not analysed quantitatively. (Note that the growth rate is not expected to drop to zero because natural convection always ensures some transfer of ions through the depleted region. Furthermore, as the electrolyte over the electrode becomes depleted, the current distribution changes so that Cu is deposited elsewhere, or other reactions, such as reduction of water, take place.)

We finally consider the effect of the finite volume of electrolyte available in the cell. In Fig. 4c,d we compare results obtained at higher growth rate with those at lower rate (Fig. 4a,b). In both cases, when the diffusion field above the electrode reaches the top of the liquid layer, we expect the growth rate to drop below that expected in the diffusion-limited regime (see note above). The situation is similar to the important case of growth in a via—a deep channel used to connect metal layers—where ions are only replenished from the end[28]. At high current density, a limiting amount of copper is deposited (Fig. 4d), consistent with significant depletion of the electrolyte above the electrode. At lower current density there is more time for additional ions to diffuse in, the initial deposition rate is maintained for longer, and the limiting thickness is three times greater. The volume from which ions can be replenished in a 2D sheet of liquid increases as $t^{1/2}$, consistent with a final thickness three times larger in the ten times slower experiment. We conclude that for the initial stages of growth at low current density, finite volume effects do become significant, but only after several seconds have passed; in other words, bulk electrodeposition can be reproduced in the cell by choosing appropriate length and timescales, and the critical initial stages are not sensitive to the limited volume.

In conclusion, we have observed the nucleation and growth of individual, nanoscale copper clusters during overpotential electrochemical deposition using a technique that allows real-time observation of liquid-phase cluster growth. On polycrystalline Au, nucleation shares characteristics of a homogeneous process with many equivalent sites available, and cluster growth is by equipartition of the available material flux over the cluster surface areas. Measurements suggest that we can reproduce conventional electrodeposition at short timescales with appropriate growth rates.

The technique developed here, with its combination of subsecond time resolution, large area of analysis and TEM analytical capabilities, is complementary to scanning-probe techniques, and is especially useful in analysing rapid 3D growth processes. We believe this technique will allow a range of electrochemical phenomena to be accessed for measurement and modelling. This includes growth on polycrystalline or patterned substrates, where spatial and temporal correlation between nucleation sites can be measured and cluster growth rates compared as a function of their environment; growth under changing conditions such as pulse plating; deposition from limited volumes of liquids as in the filling of vias; and the important effect of additives on nucleation and growth. But the technique could also open intriguing possibilities in areas such as corrosion, liquid-crystal switching dynamics, and biological materials in their active states. The cell is easily manufactured, and can be used in standard equipment widely available in academia and industry. We believe that TEM in liquid environments has the potential to enhance our knowledge of numerous processes in physics, chemistry, materials science and biology, where the ability to perform imaging and analysis at the liquid–solid interface in real-time and at small length scales is essential to gaining a deeper understanding of the phenomena involved.

METHODS

The liquid cell is made up of two Si wafers glued face to face. Each wafer is coated with 100 nm Si_3N_4 and selectively etched from the back to leave a 100 × 100 μm Si_3N_4 viewing window. A ring of SiO_2 patterned onto the lower wafer maintains a distance of 0.5–1 μm between the wafers. A polycrystalline Au working electrode is deposited across the viewing window and over a via, and connected through the wafer (resistivity 0.005 Ω cm) to an external contact. The upper wafer includes two reservoirs, which are capped with thick (1 mm) glass spacers. Liquid is introduced with a syringe and flows between the viewing windows by capillary action. The cell is then sealed by gluing sapphire lids over the holes in the spacers. A gold wire is placed as counter electrode in one reservoir, and a Cu reference electrode is placed in the other reservoir.

A heat-curing epoxy (Measurements Group, Raleigh, North Carolina) was used to glue the wafers and glass spacers, and an ultraviolet-cured epoxy (Summers Optical, Fort Washington, Pennsylvania) was used for the sapphire lids. The purpose of the glass spacers is to separate the ultraviolet-cured epoxy from the electrolyte so that the epoxy can set properly.

After loading into the microscope (a Hitachi H9000 TEM operated at 300 kV) the cell was connected to a current source. Data were recorded during galvanostatic deposition using cathodic current densities of 5 and 50 mA cm^{-2}. Galvanostatic deposition was used for *in situ* experiments because only two electrical contacts were available inside the TEM; the reference electrode was used for *ex situ* measurements. A three-electrode *in situ* system is under development allowing potentiostatic experiments to be performed. We expect an ohmic drop in the cell due to the narrow liquid channel, but this does not affect the modelling shown in the galvanostatic case.

Most images were obtained at low magnification to give a large frame size (~5 μm) and reasonable statistics for particle analysis, but frame sizes down to 500 nm could also be obtained for detailed analysis of fewer particles. To improve the image quality, an imaging energy filter (Gatan, Pleasanton, California) reduces the background of electrons scattered inelastically from the windows and liquid, and also provides spectroscopic capabilities. The number, size and position of clusters were measured in single or averaged video frames by threshholding and standard particle-counting algorithms.

The spatial resolution achievable using this technique is ~5 nm, limited by the thickness of liquid (and windows) that must be imaged[29], and 30 images can be recorded per second with high signal-to-noise ratio.

In the simulation of galvanostatic growth, clusters are nucleated at each time step, reflecting the observed constant initial nucleation rate, and grow according to equations (1) and (2). The simulation used experimentally determined macroscopic parameters, that is, the initial nucleation rate and the total growth rate, and the only free parameter was the nucleation time t_j chosen for each cluster.

Received 19 December 2003; accepted 18 June 2003; published 20 July 2003.

References

1. Volmer, M. & Weber, A. Nuclei formation in supersaturated states. *Z. Physik. Chem.* **119,** 277–301 (1926).

2. Burton, W. K., Cabrera, N. & Frank, F. C. The growth of crystals and the equilibrium structure of their surfaces. *Phil. Trans. R. Soc. Lond. A* **243,** 299–358 (1951).
3. Zhang, Z. Y. & Lagally, M. G. Atomistic processes in the early stages of thin-film growth. *Science* **276,** 377–383 (1997).
4. Rosenberg, R., Edelstein, D. C., Hu, C.-K. & Rodbell, K. P. Copper metallization for high performance silicon technology. *Annu. Rev. Mater. Sci.* **30,** 229–262 (2000).
5. Magnussen, O. M., Hotlos, J., Nickols, R. J., Kolb, D. M. & Behm, R. J. Atomic structure of Cu adlayers on Au(100) and Au(111) electrodes observed by in situ scanning tunnelling microscopy. *Phys. Rev. Lett.* **64,** 2929–2932 (1990).
6. Manne, S., Hansma, P. K., Massie, J., Elings, V. B. & Gewirth, A. A. Atomic-resolution electrochemistry with the atomic force microscope: copper deposition on gold. *Science* **251,** 183–186 (1991).
7. Bard, A. J. & Fan, F.-R. Studies of the liquid/solid interface by scanning tunneling microscopy and scanning electrochemical microscopy. *Faraday Discuss.* **94,** 1–22 (1992).
8. Schmidt, W. U., Alkire, R. C. & Gewirth, A. A. Mechanic study of copper deposition onto gold surfaces by scaling and spectral analysis of in situ atomic force microscopic images. *J. Electrochem. Soc.* **143,** 3122–3132 (1996).
9. Schneeweiss, M. A. & Kolb, D. M. Initial stages of copper deposition on Au electrodes. *Phys. Status Solidi* **173,** 51–71 (1999).
10. Hölzle, M. H., Zwing, V. & Kolb, D. M. The influence of steps on the deposition of Cu onto Au(111). *Electrochim. Acta* **40,** 1237–1247 (1995).
11. Randler, R. J., Kolb, D. M., Ocko, B. M. & Robinson, I. K. Electrochemical copper deposition on Au(100): a combined in situ STM and in situ surface x-ray diffraction study. *Surf. Sci.* **447,** 187–200 (2000).
12. Budevski, E., Staikov, G. & Lorenz, W. J. *Electrochemical Phase Formation and Growth* (VCH, Weinheim/New York, 1996).
13. Gunawardena, G., Hills, G., Montenegro, I. & Scharifker, B. Electrochemical nucleation. Part I. General considerations. *J. Electroanal. Chem.* **138,** 225–239 (1982).
14. Vereecken, P. M., Strubbe, K. & Gomes, W. P. An improved procedure for the processing of chronoamperometric data: application to the electrodeposition of Cu upon (100) n-GaAs. *J. Electroanal. Chem.* **433,** 19–31 (1997).
15. Radisic, A., Long, J. G., Hoffmann, P. M. & Searson, P. C. Nucleation and growth of copper on TiN from pyrophosphate solution. *J. Electrochem. Soc.* **148,** C41–C46 (2001).
16. Sugi, H. *et al.* Dynamic electron microscopy of ATP-induced myosin head movement in living muscle thick filaments. *Proc. Natl Acad. Sci. USA* **94,** 4378–4382 (1997).
17. Gai, P. L. Development of wet-environmental TEM for in situ studies of liquid-catalyst reactions on the nanoscale. *Microsc. Microanal.* **8,** 21–28 (2002).
18. Donnelly, S. E. *et al.* Ordering in a fluid inert gas confined by flat surfaces. *Science* **296,** 507–510 (2002).
19. Teng, H. H., Dove, P. M., Orme, C. A. & De Yoreo, J. J. Thermodynamics of calcite growth: baseline for understanding biomineral formation. *Science* **282,** 724–727 (1998).
20. Sonnenfeld, R. & Hansma, P. K. Atomic-resolution microscopy in water. *Science* **232,** 211–213 (1986).
21. LaGraff, J. R. & Gewirth, A. A. Nanometer-scale mechanism for the constructive modification of Cu single crystals and alkanethiol passivated Au(111) with an atomic force microscope. *J. Phys. Chem.* **99,** 10009–10018 (1995).
22. Keller, T. H., Rayment, T., Klenerman, D. & Stephenson, R. J. Scanning near-field optical microscopy in reflection mode imaging in liquid. *Rev. Sci. Instrum.* **68,** 1448–1454 (1997).
23. Paloczi, G. T., Smith, B. L., Hansma, P. K., Walters, D. A. & Wendman, M. A. Rapid imaging of calcite crystal growth using atomic force microscopy. *Appl. Phys. Lett.* **73,** 1658–1660 (1998).
24. Magnussen, O. M., Polewska, W., Zitzler, L. & Behm, R. J. In-situ video-STM studies of dynamic processes at electrochemical interfaces. *Faraday Discuss.* **121,** 43–52 (2002).
25. De Vries, S. A. *et al.* Surface atomic structure of KDP crystals in aqueous solution: an explanation of the growth shape. *Phys. Rev. Lett.* **80,** 2229–2232 (1998).
26. Krieger, U. K. *et al.* Rutherford backscattering to study the near-surface region of volatile liquids and solids. *Science* **295,** 1048–1050 (2002).
27. Hölzle, M. H., Apsle, C. W., Will, T. & Kolb, D. M. Copper deposition onto Au(111) in the presence of thiourea. *J. Electrochem. Soc.* **142,** 3741–3749 (1995).
28. Georgiadou, M., Veyret, D., Sani, R. L. & Alkire, R. C. Simulation of shape evolution during electrodeposition of copper in the presence of additive. *J. Electrochem. Soc.* **148,** C54–C58 (2001).
29. Reimer, L. & Gentsch, P. Superposition of chromatic error and beam broadening in transmission electron microscopy of thick carbon and organic samples. *Ultramicroscopy* **1,** 1–5 (1975).

Acknowledgements

We would like to thank S. J. Chey, M. C. Reuter and A. Ellis for valuable contributions to experimental aspects of this project, J. B. Hannon for assistance with simulations and P. Andricacos, J. M. Harper and R. G. Kelly for helpful discussions. M.J.W. and R.H. were supported through the National Science Foundation, Division of Materials Research (Focused Research Group), Grant No. 0075116.
Correspondence should be addressed to F.M.R.
Supplementary Information accompanies the paper on www.nature.com/naturematerials

Competing financial interests

The authors declare that they have no competing financial interests.

Dynamic microscopy of nanoscale cluster growth at the solid-liquid interface

MOVIES 1 AND 2: LIQUID PHASE DEPOSITION

Nucleation, growth and dissolution of Cu clusters on polycrystalline Au during electrochemical deposition and stripping. Ross-1 shows galvanostatic deposition and stripping at 5 $mAcm^{-2}$ and Ross-2 shows the same process at a higher current density of 50 $mAcm^{-2}$, in each case in an electrolyte containing 0.3M $CuSO_4$. The videos were recorded in a Hitachi H9000 TEM at 300kV using bright field imaging conditions. The field of view (horizontal distance) of 6.3 μm was chosen to give reasonable cluster statistics; smaller fields of view are possible.

In each sequence, the electron beam passes through the electrolyte, the SiN windows and the Au/Ti electrode. These contribute a uniform background. The grain size of the electrode is small (15nm) and individual grains are not visible. When the current is first applied a change of contrast occurs, caused by charging or liquid motion, but this rapidly fades and nucleation events become visible. Individual Cu clusters show as dark areas due to greater scattering allowing positions and diameters to be measured from single frames.

At 5 $mAcm^{-2}$, progressive nucleation is clearly visible and nucleation is complete after 2-3 seconds. No further growth occurs after 3 seconds due to depletion of ions in the solution. After 8 seconds the current source is turned off then a reverse (stripping) current is applied and the nuclei dissolve back into the solution.

At 50 $mAcm^{-2}$, the same processes occur but with a much shorter time scale: in this case nucleation requires less than 0.4 seconds. The nucleation density is higher and nuclei are smaller. Analysis of growth kinetics shows that depletion becomes important at an earlier time at this growth rate.

(Note - videos are shown speeded up x2 to reduce the file size.)